DESIGN AND EXPERIMENT OF TRACTION PERFORMANCE TEST EQUIPMENT FOR AGRICULTURAL TIRES
/
农用轮胎牵引性能试验设备的设计与试验

Jianguo YAN, Genglong GUO, Jiayao LI, Yaotai LI, Lijuan WANG*)
College of Mechanical and Electrical Engineering, Inner Mongolia Agricultural University, Hohhot 010018, China
Tel: +86 - 15848371910; E-mail: wanglijuan_qq@163.com
Corresponding author: Lijuan Wang
DOI: https://doi.org/10.35633/inmateh-76-89

Keywords: *agricultural tires; traction performance; tire-soil coupling; simulation analysis; field experiment*

ABSTRACT
To address the challenges of testing traction performance parameters of agricultural tires under varying soil types, tire specifications, and operational conditions, a dedicated test platform was developed to improve efficiency and reduce workload. The system includes a hydraulic drive with adjustable torque and speed, and a data acquisition module. Key components were selected based on design requirements and the frame was modeled and analyzed using ANSYS for both stress strain behavior and sixth-order modal characteristics, confirming structural integrity and absence of resonance. Field experiments were conducted using a 12.4-24 agricultural tire in accordance with the Chinese national standard GB/T 14828-2003, under three test surfaces: asphalt, withered grass field, and tilled soil. Results indicate that the developed equipment performs reliably through these conditions, demonstrating good stability and accurate data acquisition. The system's main specifications include external dimensions of 3155 mm x 1750 mm x 1385 mm, a total mass of 835.5 kg (1308.5 kg fully loaded), a variable speed range of 0-12 km/h, and a maximum driving torque exceeding 1000 N·m. These findings support the effectiveness and practical applicability of the device in agricultural tire traction performance testing.

摘要
针对农用轮胎在不同土壤类型、轮胎规格及运行条件下牵引性能参数测试存在的难题，本研究开发了一套专用试验平台系统以提高测试效率并降低工作强度。该系统配备扭矩与转速可调的液压驱动装置及数据采集模块，关键部件依据设计要求选型，并采用 ANSYS 对机架进行应力应变分析和六阶模态特性仿真，验证了结构完整性且无共振风险。按照中国国家标准 GB/T 14828-2003，选用 12.4-24 型农用轮胎在沥青路面、枯草地及翻耕地三种测试地面开展田间试验。结果表明：所研制设备在不同工况下运行可靠，稳定性良好且数据采集精确。该系统主要技术参数包括：外形尺寸 3155㎜×1750㎜×1385㎜，整机质量 835.5kg（满载 1308.5kg），测试速度范围 0-12km/h，最大驱动扭矩超 1000N·m。研究证实该装置在农用轮胎牵引性能测试中具有良好实效性与工程适用性。

INTRODUCTION
Agricultural production necessitates traction power, and the traction performance of agricultural tires, which are the primary components of wheeled agricultural machinery for achieving traction, is directly linked to the operational efficiency of such machinery *(Angelucci et al., 2025; Tekeste et al., 2023; Jjagwe et al., 2023)*. Significant energy losses occur during power transmission: studies report only 50-70% of tractor power reaches traction implements (dropping to 50% in soft soils), while 20-55% dissipates at the tire-soil interface due to rolling resistance/slippage *(Zeng et al., 2024; Farhadi et al., 2020; Kim et al 2018)*. These losses are compounded by tractor-implement compatibility issues and soil variability, causing unpredictable energy depletion *(Czarneck et al., 2019; Osinenko et al., 2015)*. Consequently, resolving tire-soil interactions is critical to mitigate slippage, fuel waste, and soil compaction *(Jasoliya et al., 2024; Małecka et al., 2024; Xi et al., 2024; Li et al., 2024)*. However, traction performance involves complex multi-factor coupling (soil type/tire parameters/operating conditions), demanding efficient testing methodologies for diverse scenario combinations *(Janulevičius et al., 2022; Zeng et al., 2025; Alkhalifa et al., 2024; Zeng et al.,2020)*.

Existing testing solutions face key limitations. Although soil-bin equipment dominates indoor research *(Taghavifar et al., 2014)* and was used in 63 studies conducted globally between 1968 and 2015 *(Ani et al., 2018)*, it inadequately replicates field conditions due to simplified soils and constrained operational parameters *(Jie et al., 2023; Kumar et al., 2019)*.

Field-capable devices often lack versatility, focusing on specific terrains like stubble fields *(Ekinci et al., 2015; Ekinci et al., 2017)*, plowed soils *(Abdolmaleki et al., 2015)*, or forest grounds *(Cudzik et al., 2018)*. In China, research is further hindered by reliance on tractor-towed systems or simulations, limiting field-validation capabilities *(Lun et al., 2016; Zhao et al., 2022; Huang et al., 2021; Wu et al., 2014)*. To address these gaps, this study develops novel traction testing equipment with four integrated innovations:

1. Self-contained operation via onboard power and steering control, enabling autonomous mobility;
2. Real-time parameter control of driving torque, speed, and wheel load through hydraulic-counterweight integration;
3. Modular single-wheel design with interchangeable tires for structural parametric studies;
4. This system uniquely supports both indoor soil-bin and field environments, overcoming prior device limitations.

The objective of this study is to design, fabricate, and experimentally validate this multifunctional equipment, establishing a standardized platform for quantifying tire-soil interactions under real-world conditions.

MATERIALS AND METHODS

Machine Structure and Operational Fundamentals

The traction performance tester consists of three main components: the frame, the power drive system, and the data acquisition system. These components are assembled as illustrated in fig. 1 (side view) and Fig. 2 (top view). The frame supports the entire test assembly rig and enables control of the travel direction via the turning mechanism. The test equipment adopts a single-wheel structure with interchangeable test tires, facilitating the study of the influence of tire structural parameters on traction performance. The power drive system includes: the diesel engine that drives the hydraulic pump, a hydraulic system, a deceleration sprocket group, and test tires. etc. This system collaboratively delivers required speed and torque outputs for tire traction testing. Driving torque is adjusted through the relief valve to control test tire torque output. Travel speed is regulated via the flow control valve to adjust the driving speed and control the slip rate of the test tires. The data acquisition system collects and processes all traction performance data from the test tires.

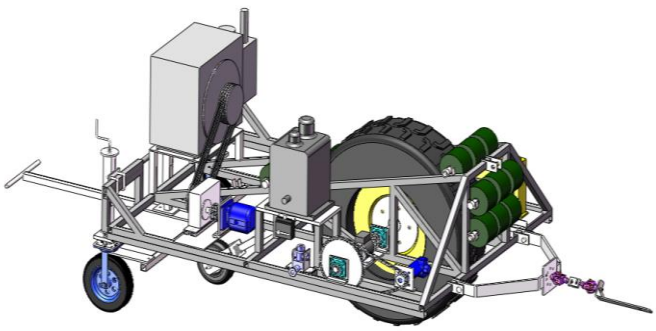

Fig. 1 - Assembly side view of agricultural tire traction performance tester

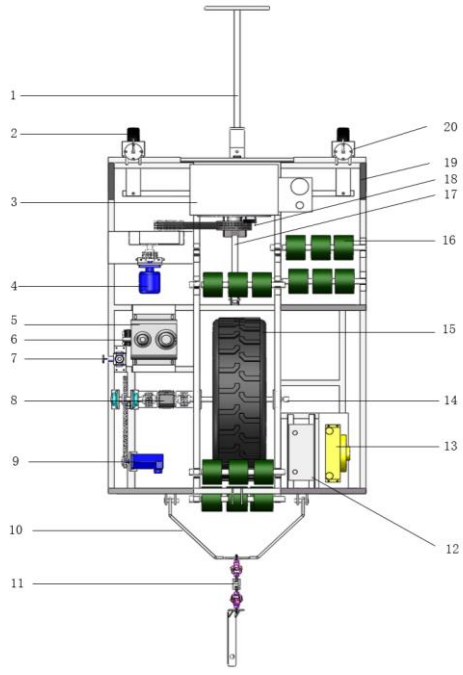

Fig. 2 - Assembly top view of agricultural tire traction performance tester

1.turning mechanism; 2.turning wheel; 3.diesel engine; 4.hydraulic pump; 5.hydraulic oil tank; 6.flow regulating valve; 7.relief valve; 8.torque sensor; 9.hydraulic motor; 10.pulling frame; 11.pulling sensor; 12.power supply; 13.hydraulic oil radiator; 14.driving wheel speed sensor; 15.test tire; 16.counterweight block; 17.driven wheel mechanism; 18.driven wheel speed sensor; 19.frame; 20.load sensor

Design of Key Components

- **Design of Frame**

The test equipment frame requires high strength and sufficient space to mount power components, test tires, and counterweights (Fig. 3(a)). The frame is constructed from 40 mm × 40 mm × 4 mm Q235 square steel welded into a grid structure. Intersecting supports ensure uniform load distribution, while triangular reinforcements at high-stress areas dissipate impacts and vibrations, guaranteeing long-term stability. Counterweight modules (three 68 kg blocks each) are fixed to the frame via angle steel (Fig. 3(b)).

The steering mechanism includes a screw lifting device, sleeve, steering wheel, and steering rod. The planar linkage mechanism (pivoted at the sleeve) is secured to both sides of the frame with U-bolts. Adjusting the steering wheel angle controls travel direction (Fig. 3(c)-(d)).

The traction mechanism comprises a traction frame, universal joints, tension sensors, and traction rods. The rods connect the tractor to the frame's suspension points via pins, enabling rolling resistance measurement under varying speeds, loads, and tire pressures (Fig. 3(e)-(f)).

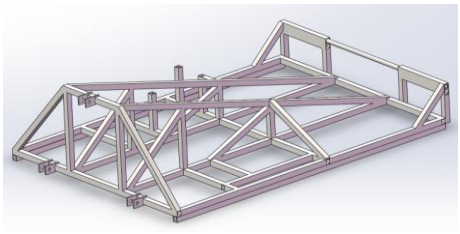

(a) Structure of frame

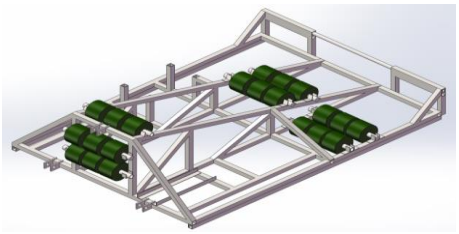

(b) Counterweights on the frame

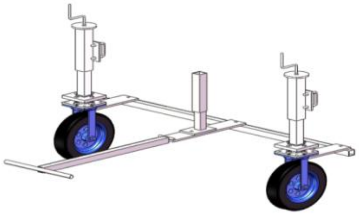

(c) Structure of turning mechanism

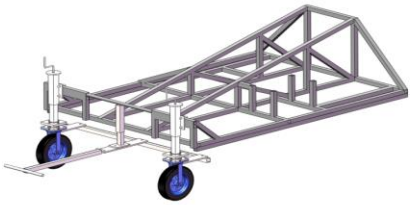

(d) Assembly scheme of turning mechanism on the frame

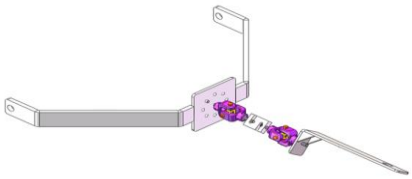

(e) Structure of pulling mechanism

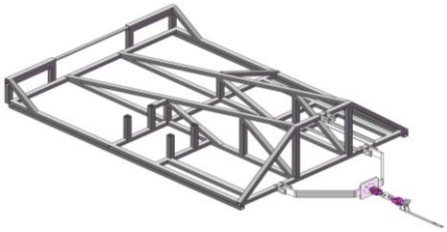

(f) Assembly scheme of pulling mechanism on the frame

Fig. 3 - Overall structure diagram of frame

- **Design of Power Drive System**

The system is primarily composed of a diesel engine, hydraulic system, reduction sprocket group, and test tires. By appropriately selecting component parameters, the system ensures that its output speed and torque meet the requirements for tire traction performance testing. The driving torque of the tire is calculated using Equation (1).

$$T_t = F_N \cdot \varphi \cdot r \cdot k \quad (1)$$

Where:

T_t is the tire driving torque (N·m), F_N is the vertical tire load (N), φ is the attachment coefficient, F_f is the rolling resistance (N), r is the tire radius, (m), k is the sliding bearing friction coefficient.

Selected 12.4-24 agricultural tires as the basis for the design of the power system; the main parameters of the tires are shown in Table 1. According to equation (1), the maximum driving torque of the test tire is calculated to be 868 N·m.

Table1

Parameters of the 12.4-24 agricultural tire

Tire Specification	Number of tire ply	Section width (mm)	Diameter (mm)	Load capacity (kg)	Maximum tire pressure (kPa)
12.4-24	8	315	1160	1415	230

The BM5-315 cycloidal hydraulic motor is selected due to its high torque density and smooth low-speed operation—critical for precise traction control in off-road testing. Its parameters are listed in Table 2. While the motor's maximum torque (900 N·m) meets requirements, its minimum speed falls short of the required 8 r/min. Therefore, a reduction sprocket assembly is integrated.

Table 2

Parameters of the BM5-315 cycloidal hydraulic motor

Type specification	Displacement (ml/r)	Maximum torque (N·m)	Speed range (r/min)	Maximum pressure (MPa)	Weight (kg)
BM5-315	296	900	15-600	20	10

The test tire 12.4-24 outer diameter is 1160 mm. To simulate the general working speed of agricultural machinery 1~15 km/h, the corresponding tire rotational speed is calculated in Equation (2):

$$n = \frac{60v}{D\pi} \tag{2}$$

where:

n is the tire rotational speed (r/min), v is the tire linear velocity (m/s), D is the diameter of the test tire (m).

To meet the tire speed requirement (4–60 r/min), a reduction device with a ratio of 3.75:1 is calculated using Equation (3).

$$i = \frac{n_1}{n_2} = \frac{Z_2}{Z_1} \tag{3}$$

Where:

i is the reduction ratio, n_1 is the input speed (r/min), take 15 r/min, n_2 is the output speed (r/min), take 4 r/min, Z_1 is the number of teeth of the main wheel, Z_2 is the number of teeth of the driven wheel,

A sprocket combination of 17 and 65 teeth is ultimately selected, providing a reduction ratio of approximately 3.8:1, which satisfies both the minimum speed and slip rate adjustment requirements.

Table 3

Parameters of JHP-2080 high pressure gear pump

Type specification	Maximum pressure (MPa)	Displacement (ml/r)	Maximum speed (r/min)	Weight (kg)
JHP-2080	25	83	2000	30

The JHP-2080 high-pressure gear pump is chosen for its volumetric efficiency and pressure stability under variable loads. Parameters are listed in Table 3. Pump displacement is calculated using Equation (4), with power demand determined via Equation (5).

$$V_2 = \frac{V_1 \cdot n_1}{n_2} \tag{4}$$

$$P = V \cdot n \cdot p \times 10^{-6} \times 1.2 \tag{5}$$

Where:

V_2 is the hydraulic pump displacement (ml/r), V_1 is the hydraulic motor displacement (ml/r), n_1 is the hydraulic motor speed (r/min), n_2 is the hydraulic pump speed (r/min), P is the hydraulic pump power (kW), V is the hydraulic pump displacement (ml/r), N is the hydraulic pump speed (r/min), p is the hydraulic pump pressure (MPa).

Based on the hydraulic pump's power demand, the ZS195 diesel engine is selected, providing robust power delivery in field environments. Specifications are detailed in Table 4.

Table 4

Parameters of ZS195 diesel engine

Type specification	Maximum power (kW)	Maximum speed (r/min)	Sizes (mm)	Weight (kg)
ZS195	10.8	2200	830×380×670	145

The hydraulic system consists of a hydraulic oil tank, hydraulic pump, relief valve, flow control valve, bidirectional hydraulic motor, and temperature-controlled electronic radiator. The principle of the hydraulic system is shown in Fig. 4. The diesel engine drives the hydraulic pump, which delivers hydraulic oil through a filter to the hydraulic motor, producing output speed and torque that meet performance requirements. The system regulates driving torque via the relief valve, adjusts speed through the flow control valve, and maintains normal hydraulic oil temperature using the temperature-controlled radiator, ensuring continuous operation and system stability.

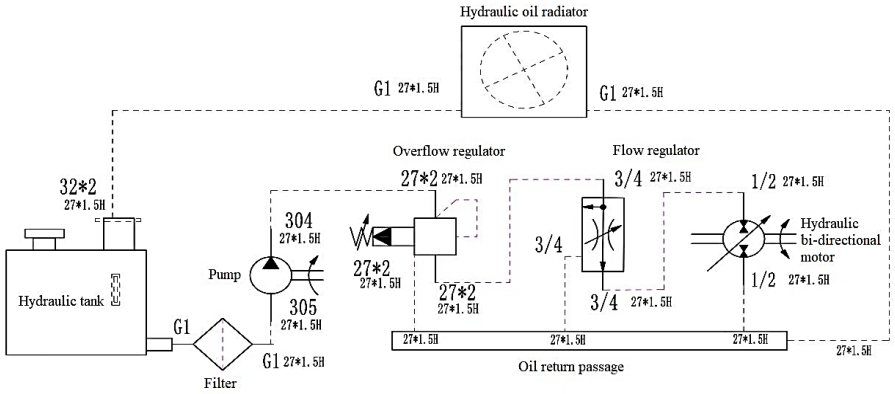

Fig. 4 - Hydraulic schematic diagram

● Design of Data Acquisition System

The system architecture consists of sensors, a data acquisition processor, a communication module, and a central PC interface. Sensors include a test tire RPM sensor and following wheel RPM sensor (both connected directly to the data acquisition processor's input ports), along with a torque sensor, left/right turning wheel load sensors, and a pulling sensor – these are connected to the processor's input ports via transmitters. The data acquisition processor collects and processes signals from all sensors before transmitting the output data through an RS232 serial communication interface to the central PC. The PC then receives and displays all measurement data in real time. Power is supplied to all sensors and the data acquisition processor by a dedicated power management module.

According to the RPM speed requirements of the tester power drive system, the DW3806 RPM sensor is selected (Fig. 5(a)), with parameters detailed in Table 5. The tire RPM sensor measures the rotational speed of the driven tire, while the follower wheel RPM sensor determines the actual linear travel speed of the platform. This configuration enables slip calculation by comparing theoretical travel speed (derived from driven tire rotation) with actual linear movement. The tire RPM sensor is installed at the end of the tire drive shaft (Fig. 5(b)), and the follower wheel RPM sensor is mounted at the end of the follower wheel shaft (Fig. 5(c)). Both sensors are coupled to their respective shafts via winding couplings, with mounting positions secured by positioning plates.

Table 5

Parameters of the DW3806 RPM sensor

Para-meters	Dimensions (OD mm x H mm)	Shaft diameter (mm)	Radial load (N)	Axial load (N)	Starting torque (N·m)	Maximum speed (r/min)	Moment of inertia (g/cm^2)	Allowable angular acceleration (rad/s)	Weight (kg)
Value	37 x 52	6	≤30	≤20	≤2×10^{-3}	6000	20	2 x 10^4	0.1

(a) RPM sensor *(b) Test tire RPM sensor* *(c) Following wheel RPM sensor*

Fig. 5 - RPM sensor and assembly scheme

The torque sensor is used to test the driving torque of the test tire, installed on the tire drive shaft. According to the output torque designed for the power drive system of the tester, the JN-DN4 torque sensor is selected for its ability to provide accurate real-time measurement to test the driving torque of the test tire, and the relevant parameters of the torque sensor are shown in Table 6. In order to achieve the purpose of real-time measurement during operation, the sensor is fixed between the sprocket power output shaft and the drive tire shaft, and both sides are connected through roller chain coupling, as shown in Fig. 6.

Table 6

Parameters of JN-DN4 torque sensor

Parameters	Overall dimensions (L mm × W mm × H mm)	Shaft diameter (mm)	Range (N·m)	Combined accuracy (%)	Rated speed (r/min)	Maximum speed (r/min)	Safe overload (%)	Operating environment (℃)
Value	230 x 127 x 168.5	38	0~5000	± 0.3	4000	6000	120	-10~+60

(a) Torque sensor

(b) Torque sensor assembly scheme

Fig. 6 - Torque sensor and assembly scheme

The left and right turning wheel load sensors are used to test the loads of the left and right turning wheels, which are used to calculate the actual loads of the tire under test, and are mounted between each ground wheel and the bottom of the test frame. The full load weight of the test set is about 1308.5 kg, and the overall weight is borne by the driving tire and the two turning wheels, with the test tire as the main load-bearing wheel. The ZNLBU-I load cell is selected due to its robust design and suitability for the anticipated load range to measure the load of the turning wheels, as shown in Fig. 7(a), and the relevant parameters of the load cell are shown in Table 7. In order to facilitate the disassembly and installation of the cell and the load test, the upper mounting plate can slide up and down through the positioning guide pillar, and the turning wheel rotor shaft is provided with a structure for mounting the load cell, as shown in Fig. 7(b). This mounting structure allows for straightforward calibration and maintenance.

Table 7

Parameters of ZNLBU-I load sensor

Parameters	Overall dimensions (O.D. mm × H. mm)	Range (kg)	Sensitivity (mv/V)	Combined accuracy (%)	Operating temperature range (°C)	Thread size (mm)	Allowable overload (%)	Sealing grade
Value	72 x 27	600	1.2	0.05	-20~+70	M12×1.75	120	IP66

(a) Load sensor

(b) Load sensor assembly scheme

Fig. 7 - Load sensor and assembly scheme

A pulling sensor is used to test the rolling resistance of the tire under test. According to the rolling resistance estimation under the maximum load of the test tire, it is determined that the ZNLBS-I pulling sensor

is selected, as its measurement range and accuracy are appropriate for the expected rolling resistance forces, as shown in Fig. 8 (a). The parameters of the sensor are shown in Table 8, and the sensor is mounted on the pulling bar during the towing test and coupled with the pulling mechanism of the tractor, as shown in Fig. 8 (b).

Table 8

Parameters of ZNLBS-I pulling sensor

Parameters	Dimensions (L mm x W mm x H mm)	Range (N)	Sensitivity (mv/V)	Operating temperature range (°C)	Thread Size (mm)	Allowable overload (%)	Sealing Grade
Value	51 x 19 x 76	5000	2	-20~+70	M12×1.75	150	IP67

(a) Pulling sensor *(b) Pulling sensor assembly scheme*

Fig. 8 - Pulling sensor and assembly scheme

The circuit diagram of the data acquisition system is shown in Fig. 9. A 24 V lithium battery pack powers the system for sustained outdoor operation, simultaneously supplying the data acquisition processor and all sensors. Voltage regulators mitigate battery voltage fluctuations, while a fuse protects against short circuits or overloads. The rotational speed sensors' encoders generate pulse signals (sampled at 1 kHz with ±0.1% accuracy) from the test tire and follower wheel axles, transmitted to the PLC's X0–X3 high-speed input ports. Analog-output sensors (left/right wheel load, torque, and pulling sensors) convert physical quantities to voltage signals (0–10 V range, 16-bit resolution), routed to the PLC's AD0–AD3 ports for synchronized analog-to-digital conversion at 500 Hz. All channels are sampled simultaneously via PLC scan-cycle synchronization to ensure temporal alignment for slip/force calculations. Processed data is sent via RS232 to a Human Machine Interface (HMI) for real-time numerical display, enabling intuitive monitoring. A USB interface facilitates data download for post-processing.

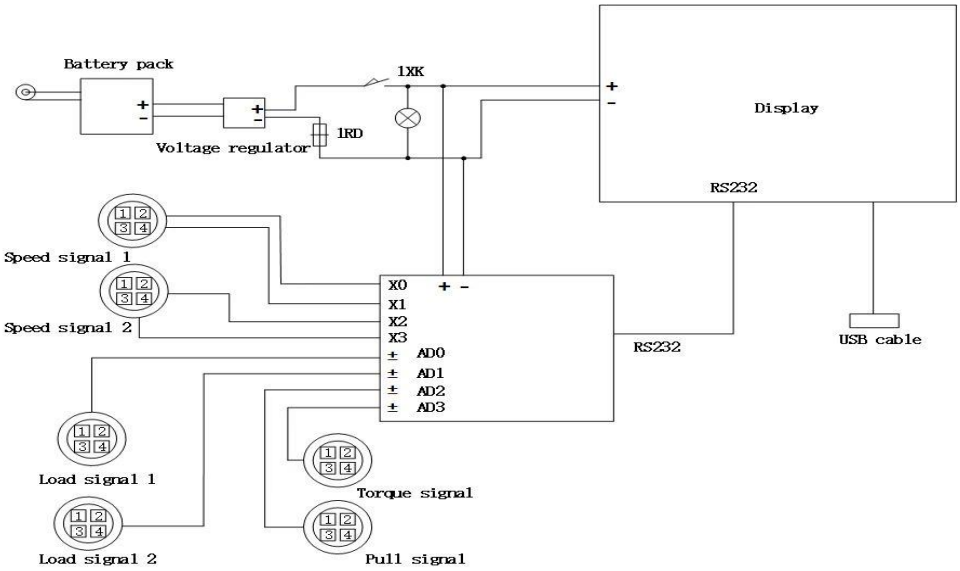

Fig. 9 - Circuit diagram of data acquisition system

The designed and fabricated data acquisition instrument is shown in Fig. 10(a), and the working interface of the data acquisition instrument is shown in Fig. 10(b). The data acquisition instrument is used to display and save the output of each sensor test data.

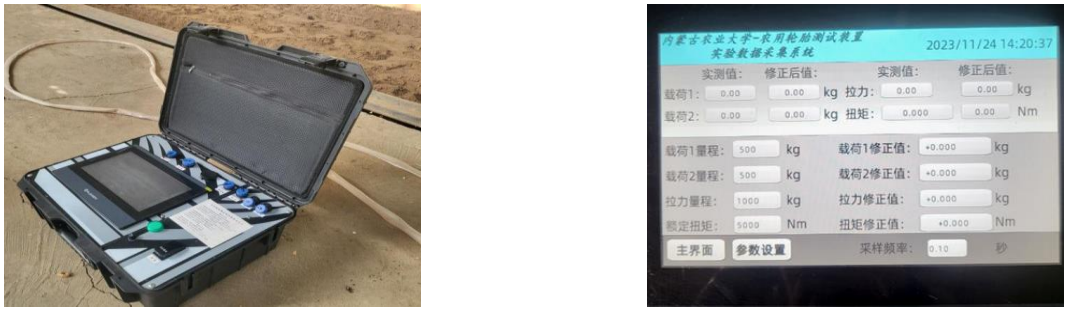

(a) Data acquisition instrument *(b) Working interface of data acquisition instrument*

Fig. 10 - Data acquisition instrument and working interface

The designed systems were integrated, and the developed agricultural tire traction performance test equipment is shown in Fig.11.

Fig. 11 - Agricultural tire traction performance test equipment

Experiment Scheme

- **Simulation Experiment**

ANSYS was used for carrying out static analysis of the frame to check whether the strength of the frame meets the requirements. In addition, the frame is installed with a diesel engine driving the hydraulic pump. In order to check whether the coercive vibration generated in the operation of the engine will cause resonance problems in the frame, modal analysis of the frame is needed.

By elucidating the dynamic characteristics and vibrational modes of the equipment, modal analysis facilitates the identification of critical frequencies and potential resonance points that could adversely affect the precision and reliability of traction measurements. SolidWorks software is used to establish a three-dimensional structural model of the frame, and the frame model is imported into ANSYS Workbench to construct a finite element model. The material of the frame is Q235A carbon structural steel, and the relevant mechanical parameters are listed in Table 9. The two bearing surfaces of the test tires and the mounting plates of the two steering wheels are defined as "fixed supports" in the fixed support setting. The overall load on the frame is distributed between the fuel tank $(24\ \mathrm{kg})$, the diesel engine $(145\ \mathrm{kg})$, hydraulic pump $(30\ \mathrm{kg})$, hydraulic motor $(10\ \mathrm{kg})$, electric battery $(18\ \mathrm{kg})$, hydraulic oil radiator and fan $(15\ \mathrm{kg})$, and 7 sets of counterweights $(7 \times 68\ \mathrm{kg})$ are applied, so the frame force is the gravity of each of these components. The setup applies loads to each of the above components at the corresponding mounting part of the frame and performs the computational solution.

Table 9

Material properties of Q235A

Material	Density (kg/m^3)	Young's modulus (Pa)	Yield strength (Pa)	Tangent modulus (Pa)	Poisson's ratio
Q235A	7860	2.12 x 10^{11}	2.35 x 10^8	6.1 x 10^9	0.288

● **Field Experiment**

A field experiment covering three aspects was conducted to verify whether the working performance of the developed tester could meet the expected goals. Firstly, test the ability of the test equipment to work stably, including the stability of the travel speed and the ability to adapt to the work of different terrain conditions. Secondly, according to the Chinese national standard "GB_T14828-2003 Agricultural Tire Traction Performance Test Method," the relationship between tire tractive efficiency and slip rate with traction coefficient under different terrain conditions was investigated. Finally, a field experiment was carried out to investigate the effects of tire load and pressure on traction force and rolling resistance under different terrain conditions.

The experiment was conducted at the experimental base of Inner Mongolia Agricultural University. The asphalt road, withered grass field, and tillage were selected as the terrain conditions, as shown in Fig. 12. The experiment was conducted in October 2024. The soil parameters of withered grass fields and tillage are shown in Table 10.

(a) Asphalt road

(b) Withered grass field

(c) Tillage

Fig. 12 - Three experimental terrain conditions

Table 10

Soil parameters of withered grass field and tillage

Withered grass field		Tillage	
parameter	**value**	**parameter**	**value**
Moisture content (%) (0-20 cm)	3-5	Moisture content (%) (0-20 cm)	16-18
Penetration resistance ($N \cdot cm^{-2}$) (0-20cm)	312.4	Penetration resistance ($N \cdot cm^{-2}$) (0-20cm)	135.2
Shearing strength ($kN \cdot m^{-2}$)	36.91	Shearing strength ($kN \cdot m^{-2}$)	7.89

Experiment of the stable working capacity of the tester:

In order to verify the stability of the travel speed of the tester and its adaptability to work under three kinds of terrain conditions, the tester was maneuvered to travel more than 50 meters under the conditions of loaded 340 kg counterweight block (full load 13085 N) and unloaded counterweight (8355 N). A total of 16 sets of speed data were tested on each kind of terrain, including 8 sets under the conditions of full load and 8 sets under the conditions of unloaded counterweight. In the test, the turning mechanism controls the tester to keep traveling in a straight line as far as possible. The travel speed of the test tire was changed by the flow-regulating valve in the hydraulic system. The data collection was started after the travel speed of the tester was stabilized in each test. The travel speed of the tester was measured by the following wheel speed sensor. At the same time, the GPS-based VBOX data acquisition system (produced by RaceLogic, UK, with a speed measurement accuracy of 0.1km/h) was used for measuring the travel speed of the tester. The travel speed stability and terrain adaptation ability of the tester were evaluated by comparing the difference in speed between the two measurements.

(2) Experiment on the traction performance of agricultural tire based on Chinese national standard GB_T14828-2003:

According to the "GB_T14828-2003 test method for traction performance of agricultural tires" (*GB/T 14828-2003*), the experiment on the relationship between the slip rate of agricultural tires, tractive efficiency, and traction coefficient was carried out, which could check whether the driving torque of the tester and the adjusting range can meet the test requirements.

The calculations of tire slip rate S, tractive efficiency TE, and traction coefficient TC are shown in Equations (6)-(10):

$$\text{Tire travel reduction (S).}\ S = (1 - \frac{v_a}{v_t}) \times 100\% \quad (6)$$

$$\text{Traction coefficient}\ TC = \frac{F_t}{G} \quad (7)$$

$$\text{Drawbar power.}\ P_D = F_t \cdot v_a \quad (8)$$

$$\text{Axle power (kW).}\ P_a = \frac{T \cdot n}{9550} \quad (9)$$

$$\text{Tractive efficiency.}\ TE = \frac{P_D}{P_a} \times 100\% \quad (10)$$

where:

v_a is the tire actual velocity (m/s), v_t is the tire theoretical velocity (m/s), F_t is the traction force of tire (N), G is the vertical load of tire (N), T is the tire axle torque (N.m), n is the tire rotation speed (rpm).

The relief valve of the hydraulic system was used to adjust the driving torque of the test tire. As the driving torque of the test tire increases gradually from small to large, the traction coefficient increases with the driving torque of the tire. As the traction coefficient increases, the slip component of the tire roll increases gradually, and the tire tractive efficiency will also change.

Therefore, by carrying out the agricultural tire traction performance experiment, it was examined whether the tester could complete the tire traction test under the three different terrain conditions according to the Chinese national standard GB_T14828-2003.

(3) Experiment on the effect of tire load and pressure on tire traction performance:

The effect of tire load and pressure on rolling resistance and traction was investigated under three terrain conditions. The tire load was adjusted by using counterweights, and the vertical loads of the tire were 8355 N, 10395 N, 11755 N, and 13085 N, respectively, while the tire pressure was set to 120 kPa. The tire pressure could be adjusted by inflation and deflation, and the tire pressure was set to 80 kPa, 120 kPa, 160 kPa, and 200 kPa, respectively. At the same time, the tire load was set to 8355 N. The travel speed of the tester was kept stable during the test, and the test was repeated three times under each test condition, and the average value of the data from the three repeated tests was taken as the final test value. The average travel speeds of the tester measured during the tests on asphalt roads, field withered grass, and tillage were 3.56 km/h, 3.25 km/h, and 2.51 km/h, respectively.

RESULTS AND ANALYSIS

Analysis of Simulation Results

Through static analysis, the frame exhibits a maximum total deformation of 0.53963 mm at the diesel engine mounting plate (Fig. 13a) and a maximum equivalent stress of 79.248 MPa at the engine mounting holes and counterweight block groove (Fig. 13b). This deformation magnitude is functionally acceptable since, under dynamic field conditions (e.g., tractor-induced vibrations exceeding ±3 mm per ISO 5008), the 0.53963 mm static deflection is negligible relative to system-level displacements. The material of the frame is Q235A. The Q235A steel frame's maximum stress (79.248 MPa) remains below the material's 235 MPa yield strength (GB/T 700-2006), confirming a safety factor >2.96. Thus, the frame's structural adequacy is validated for all operational scenarios.

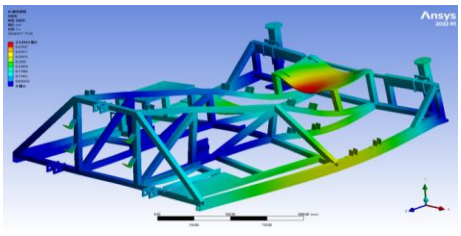

(a) Deformation cloud image of the frame

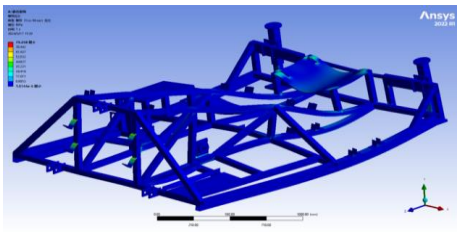

(b) Equivalent stress cloud image of the frame

Fig. 13 - Deformation cloud and equivalent stress cloud image of the frame

Modal analysis confirmed the structural integrity of the frame under dynamic loads. Table 11 lists the first six orders of intrinsic frequencies obtained through solving the frame modes. Fig. 14 presents the results of the first six-order modal analysis. The natural frequencies differ across orders, resulting in correspondingly distinct deformations of the frame at each frequency. Higher deformation amplitudes occurred at the mounting points (diesel engine, oil tank, hydraulic pump, counterweight), exhibiting reciprocating and torsional deformation modes.

Table 11

Intrinsic frequencies of the first 6 orders of modes of the frame

Order	1	2	3	4	5	6
Intrinsic frequency value (Hz)	26.389	42.769	52.076	56.613	62.348	67.081

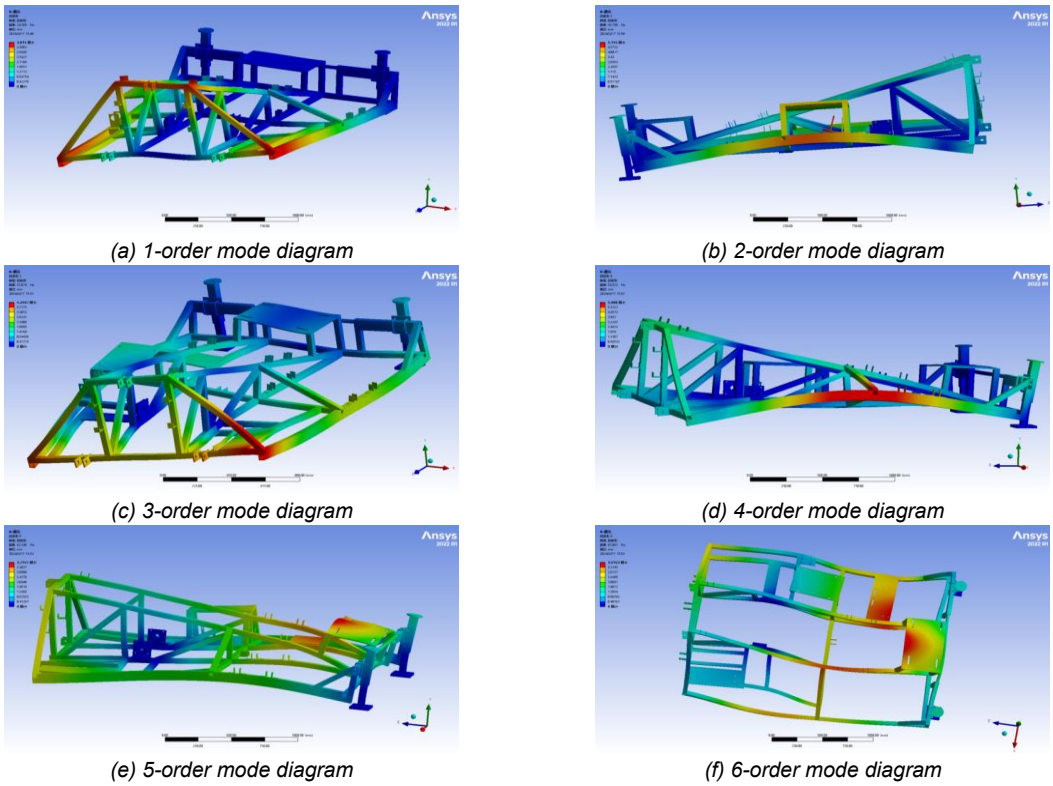

(a) 1-order mode diagram (b) 2-order mode diagram

(c) 3-order mode diagram (d) 4-order mode diagram

(e) 5-order mode diagram (f) 6-order mode diagram

Fig. 14 - First 6 order modal diagram of the frame

The main vibration excitation to the frame is from the vibration generated by the operation of the diesel engine. The selected diesel engine is a single-cylinder 4-stroke engine, and the engine excitation frequency is calculated as Equation (11):

$$f = \frac{2nz}{60k} \tag{11}$$

where:

f is the engine excitation frequency (Hz), n is the engine speed (r/min), z is the number of engine cylinders, k is the number of engine strokes.

The engine idle speed is 800 r/min, so the excitation frequency of the engine is calculated to be 6.67 Hz. The maximum speed of the engine is 2200 r/min, and the vibration frequency is 18.33 Hz. It can be seen from Table 10 that the lowest intrinsic frequency of the frame is 26.389 Hz, which is higher than the maximum excitation frequency of the engine. So, there is no resonance occurring in the frame. While the magnitude of deformation increases with the modal order, all values remain within safe limits.

Analysis of Field Experiment Results

- **Experiment of the stable working capacity of the tester**

The test results of the tester in three terrain conditions with different travel speeds are shown in Fig. 15.

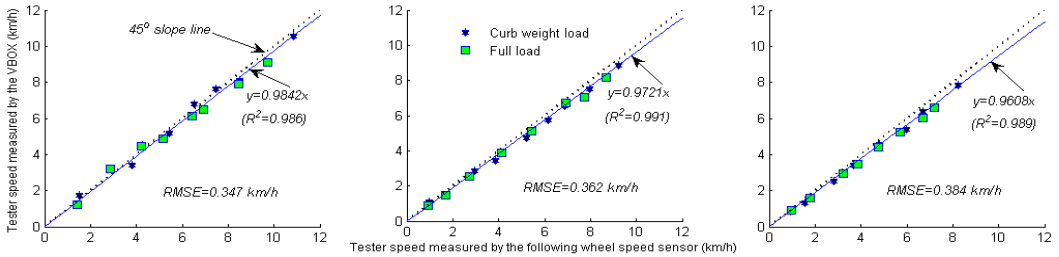

(a) Asphalt road *(b) Withered grass field* *(c) Tillage*

Fig. 15 - Test results for different travel speeds

As shown in Figure 15, the travel speeds measured by the tester's RPM sensor and the VBOX reference system show good agreement under both curb weight and full load conditions. RMSE values were 0.347 km/h (asphalt), 0.362 km/h (withered grass), and 0.384 km/h (tillage). A consistent minor overestimation by the RPM sensor (<0.4 km/h RMSE), attributed to wheel bounce on rough terrain, is operationally negligible. This discrepancy does not impact core functions (stability assessment, maneuverability) and falls within acceptable tolerances for agricultural machinery testing.

- **Experiment on the traction performance of agricultural tire based on national standard GB_T14828-2003**

The experimental results of tire tractive efficiency and slip rate versus traction coefficient are shown in Fig. 16.

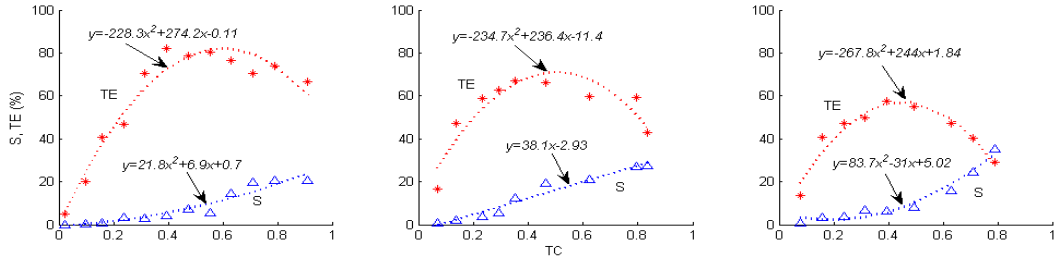

(a) Asphalt road *(b) Withered grass field* *(c) Tillage*

Fig. 16 - Relationship between tractive efficiency TE, slip rate S and traction coefficient TC

As can be seen from Fig. 16, under the three terrain conditions, tire tractive efficiency and slip rate vary with traction coefficient, but the trends are basically the same. That is, the slip rate increases with the increase of the traction coefficient, and the tractive efficiency increases and then decreases with the increase of the traction coefficient, which conforms to the trend of the relationship between the tractive efficiency and slip rate with the traction coefficient in GB_T14828-2003. It shows that the driving torque output characteristics and adjustment range of the tester can meet the road and field test environment and can be used to carry out agricultural tire traction performance tests, which lays a foundation for the study of tire-soil coupling mechanisms.

- **Experiment on the effect of tire load and pressure on tire traction performance**

Based on the analysis of the test data, the effects of load and tire pressure on the tire traction force are shown in Fig. 17, and the effects of load and tire pressure on the rolling resistance of the tire are shown in Fig. 18.

(a) Effect of load on tire traction *(b) Effect of tire pressure on tire traction*

Fig. 17 - Effect of Load and Tire Pressure on Tire Traction

From Fig. 17(a), it can be seen that the traction force of a tire at the same load is the largest on an asphalt road and the smallest on tillage. The traction force of agricultural tires traveling on asphalt roads, withered grass fields and tillage is increasing as the tire load increases from 8355 N to 13085 N. This is consistent with the conclusion obtained through experimental data fitting in reference (*Zhu et al., 2020*), that is, the traction force of the tire increases with the increase of vertical load on the axle. In addition, compared with tillage, the traction force of tires traveling on asphalt roads and withered grass fields increases more significantly with the increase in load.

From Fig. 17(b), it can be seen that with the increase of tire pressure from 80 kPa to 200 kPa, the traction force of agricultural tires traveling on asphalt roads, withered grass fields and tillage decreases gradually, among which the traction force traveling on tillage decreases more obviously with the increase of tire pressure. Zhu et al. investigated the effect of the tire vertical load with the tire pressure on tractor traction performance. The results show that the tire traction force is linearly related to the vertical load on the axle, the maximum traction force of the tire is somewhat linearly related to the vertical load on the axle, and the tire deformation displacement increases with the increase of the tire driving force. With the increase of vertical load and the decrease of tire pressure, the adhesion performance of the tire is improved.

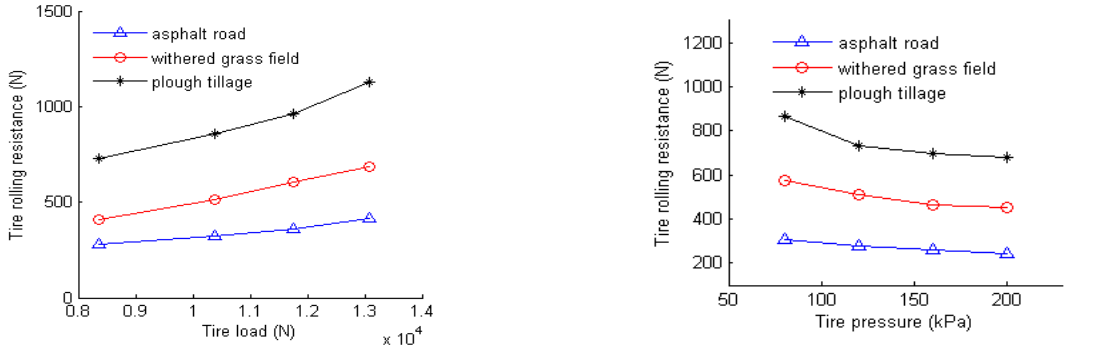

(a) Effect of load on tire rolling resistance *(b) Effect of tire pressure on tire rolling resistance*

Fig. 18 - Effect of load and tire pressure on tire rolling resistance

From Fig. 18(a), it can be seen that the rolling resistance of tires on tillage is the largest and the rolling resistance on asphalt roads is the smallest for the same load. The rolling resistance of agricultural tires running on asphalt roads, withered grass fields and tillage is increasing as the tire load is increased from 8355 N to 13085 N. The rolling resistance of agricultural tires running on asphalt roads and asphalt roads is increasing with increasing load. The increase in rolling resistance with increasing load is more pronounced for tires running on tillage compared to asphalt roads and withered grass fields.

As can be seen from Fig. 18(b), the rolling resistance of agricultural tires running on asphalt roads, withered grass fields and tillage decreases gradually as the tire pressure increases from 80 kPa to 200 kPa. The rolling resistance of running on the tillage decreases more obviously with the increase of the tire pressure. By means of an experimental method, *Čiplienė et al., (2019*), investigated the effect of front and rear tire pressure combinations on tractor traction performance. The results showed that a traction advantage of about 2% could be produced by setting the front and rear tire pressure combinations appropriately.

CONCLUSIONS

In this study, an agricultural tire traction performance tester was designed. The structure parameters and the key components of the frame, the power drive system, and the data acquisition system were determined. The tester can be used to carry out experimental tests in indoor soil tanks and fields for testing traction performance parameters such as rolling resistance, traction force, slip rate, traction efficiency and traction power consumption of agricultural tires. The tester adopts a single tire structure and can replace different specifications of the test tire. Also, the tester comes with a power source to achieve self-propelled function. The turning mechanism is designed to achieve control of the traveling direction. Most importantly, a wide range of test conditions can be generated depending on tire parameters, soil type, and driving conditions.

Taking 12.4-24 agricultural tire as the test object, according to Chinese national standard "GB_T14828-2003 test method for traction performance of agricultural tires," the experiment was conducted under asphalt roads, withered grass fields and tillage conditions. The travel speeds of the tester measured by the RPM sensor of the tester and the travel speeds measured by the VBOX are in good agreement, both under the conditions of curb weight load and full load. The RMSE values for travel speeds on asphalt roads, withered grass fields and tillage are 0.347 km/h, 0.362 km/h and 0.384 km/h, respectively. The results verified that the tester has the ability to work stably, including the stability of travel speed and the ability to adapt to different terrain conditions. The driving torque output characteristics and adjustment range of the tester can meet the road and field test environment, which indicates that the design of the tester is scientific and practical. That lays the foundation for the subsequent in-depth research on the mechanism of agricultural tire-soil coupling. It is important to note that when conducting experimental operations using this equipment, direction control is essential. When the speed exceeds 5 km/h, a sufficiently long test section must be allocated. Particularly when conducting experiments in indoor soil bins, the test speed should be appropriately regulated based on the length of the soil bin to ensure the safety of both the equipment and the operating personnel.

In future research, this equipment will be utilized to conduct traction performance tests for agricultural tires, aiming to investigate the coupling mechanism between agricultural tires and various types of farmland soil. Based on soil conditions, the study will propose the optimal matching relationship between tire structural parameters and operating conditions to achieve efficient and low-energy-consumption traction behavior. This research will provide a basis for the rational selection of agricultural tires and the effective regulation of their traction performance.

ACKNOWLEDGEMENT

This research was funded by the National Natural Science Foundation of China (52362056), Inner Mongolia Natural Science Foundation (2023LHMS05006), Inner Mongolia Natural Science Foundation (2025MS05131), the Program for improving the Scientific Research Ability of Youth Teachers of Inner Mongolia Agricultural University (BR230126), and Inner Mongolia Autonomous Region “First-Class Discipline Research Special Project” (Creation of Intelligent Equipment for the Whole Industrial Chain of Grass Industry and Special Economic Mixed Grain, No. YLXKZX-NND-046).

REFERENCES

[1] Angelucci, L., Pinet, F., Vertua, A., & Mattetti, M. (2025). Towards more efficient tractors: Assessing and refining traction test procedures for agricultural tractors. *Journal of Terramechanics*, Vol.117, pp.101018, Italy. https://doi.org/10.1016/j.jterra.2024.101018

[2] Tekeste, M. Z., Way, T. R., Birkenholz, W., & Brodbeck, S. (2023). Effect of increased deflection tire technology on soil compaction. *Journal of the ASABE*, Vol.66, issue 1, pp.75-84, American. https://doi.org/10.13031/2013.21335

[3] Jjagwe, P., Tekeste, M. Z., Alkhalifa, N., & Way, T. R. (2023). Modeling tire-soil compression resistance on artificial soil using the scaling law of pressure-soil sinkage relationship. *Journal of Terramechanics*, Vol.108, pp.7-19, USA. https://doi.org/10.1016/j.jterra.2023.02.002

[4] Zeng, H., Tang, X., Chen, S., & Qi, H. (2024). Numerical investigations of traction behaviors of a pneumatic tire on wet granular terrains: DE/FE simulations. *Journal of Terramechanics*, Vol.113, pp.10-22, China. https://doi.org/10.1016/j.jterra.2024.100972

[5] Farhadi, P., Golmohammadi, A., Malvajerdi, A. S., & Shahgholi, G. (2020). Tire and soil effects on power loss: Measurement and comparison with finite element model results. *Journal of Terramechanics*, Vol.92, pp.13-22, Iran. https://doi.org/10.1016/j.jterra.2020.09.004

[6] Kim, Y. S., Lee, S. D., Kim, Y. J., Kim, Y. J., & Choi, C. H. (2018). Effect of tractor travelling speed on a tire slip. *Korean Journal of Agricultural Science*, Vol.45, issue 1, pp.120-127, Korea. https://doi.org/10.7744/kjoas.20180002

[7] Czarnecki, J., Brennensthul, M., Białczyk, W., Ptak, W., & Gil, Ł. (2019). Analysis of traction properties and power of wheels used on various agricultural soils. *Agricultural Engineering*, Vol.23, issue 1, pp.13-23, Poland. doi:10.1515/agriceng-2019-0002. https://doi.org/10.1515/agriceng-2019-0002

[8] Osinenko, P. V., Geissler, M., & Herlitzius, T. (2015). A method of optimal traction control for farm tractors with feedback of drive torque. *Biosystems engineering*, Vol.129, pp.20-33, Germany. https://doi.org/10.1016/j.biosystemseng.2014.09.009

[9] Jasoliya, D., Untaroiu, A., & Untaroiu, C. (2024). A review of soil modeling for numerical simulations of soil-tire/agricultural tools interaction. *Journal of Terramechanics*, Vol.111, pp.41-64, USA. https://doi.org/10.1016/j.jterra.2023.09.003

[10] Małecka, A., Brennensthul, M., Ptak, W., Czarnecki, J., & Lejman, K. (2024). Evaluation of the Changes in Dimensions of the Footprint of Agricultural Tires under Various Exploitation Conditions. *Applied Sciences*, Vol.14, issue 12, pp.5228, Poland. https://doi.org/10.3390/app14125228

[11] Xi, Z., Feng, T., Liu, Z., Xu, H., Zheng, J., & Xu, L. (2024). Estimation of Soil Characteristic Parameters for Electric Mountain Tractor Based on Gauss–Newton Iteration Method. *World Electric Vehicle Journal*, Vol.15, issue 5, pp.217, China. https://doi.org/10.3390/wevj15050217

[12] Li, S., Wu, J., Wan, Y., Su, B., & Wang, Y. (2024). Numerical Study of Tangential Traction Mechanism between Pattern Blocks of Agricultural Radial Tires and Soft Soil. *Materials*, Vol.17, issue 16, pp.1-18, China. https://doi.org/10.3390/ma17163906

[13] Janulevičius, A., & Damanauskas, V. (2022). Prediction of tractor drive tire slippage under different inflation pressures. *Journal of Terramechanics*, Vol.101, pp.23-31, Lithuania. https://doi.org/10.1016/j.jterra.2022.03.001

[14] Zeng, H., Lin, Z., Huang, G., Yang, X., Li, Y., Su, J., & Xu, W. (2025). Parameter identification of DEM-FEM coupling model to simulate traction behavior of tire-soil interaction. *Journal of Terramechanics*, Vol.117, pp.101012, China. https://doi.org/10.1016/j.jterra.2024.101012

[15] Alkhalifa, N., Tekeste, M. Z., Jjagwe, P., & Way, T. R. (2024). Effects of vertical load and inflation pressure on tire-soil interaction on artificial soil. *Journal of Terramechanics*, Vol.112, pp.19-34, USA. https://doi.org/10.1016/j.jterra.2023.11.002

[16] Zeng, H., Xu, W., Zang, M., & Yang, P. (2020). Experimental and numerical investigations of tractive performance of off-road tires on gravel terrain. *International Journal of Computational Methods*, Vol.17, issue 08, pp.1950055, China. https://doi.org/10.1142/S0219876219500555

[17] Taghavifar, H., & Mardani, A. (2014). Analyses of energy dissipation of run-off-road wheeled vehicles utilizing controlled soil bin facility environment. *Energy*, Vol.66, pp.973-980, Iran. https://doi.org/10.1016/j.energy.2014.01.076

[18] Ani, O.A., Uzoejinwa, B.B., Ezeama, A O., Onwualu, A.P., Ugwu, S.N., & Ohagwu, C.J. (2018). Overview of soil-machine interaction studies in soil bins. *Soil and Tillage Research*, Vol.175, issue 1, pp.13-27, Nigeria. https://doi.org/10.1016/j.still.2017.08.002

[19] Wang, J., Shang, L., Xu L., & Tang Q. (2023). Evaluation of traction characteristics of tractor tires on loose soils: simulation and experimental research. *INMATEH-Agricultural Engineering*, Vol.71, issue 3, pp.379-390, https://doi.org/10.35633/inmateh-71-33

[20] Kumar, S., Noori, M. T., & Pandey, K. P. (2019). Performance characteristics of mode of ballast on energy efficiency indices of agricultural tyre in different terrain condition in controlled soil bin environment. *Energy*, Vol.182, issue 1, pp.48-56, India. https://doi.org/10.1016/j.energy.2019.06.043

[21] Ekinci, Ş., Çarman, K., & Kahramanlı, H. (2015). Investigation and modeling of the tractive performance of radial tires using off-road vehicles. *Energy*, Vol.93, issue 2, pp.1953-1963, Turkey. https://doi.org/10.1016/j.energy.2015.10.070

[22] Ekinci, Ş., & Çarman, K. (2017). Effects of some properties of drive tires used in horticultural tractors on tractive performance. *Journal of Agricultural Sciences*, Vol.23, pp.84-94, Turkey.

[23] Abdolmaleki, H., Jafari, A., Tabatabaeifar, A., Hajiahmad, A., & Goli, H. (2015). Development and evaluation of an in-situ tire testing facility with variable side slip angles. *Journal of Terramechanics*, Vol.59, pp.49-58, Iran. https://doi.org/10.1016/j.jterra.2015.03.002

[24] Cudzik, A., Brennensthul, M., Białczyk, W., & Czarnecki, J. (2018). Tractive performance of tyres in forest conditions–impact assessment of ground and tyres parameters. *Croatian Journal of Forest Engineering*, Vol.39, issue 1, pp.85-96, Poland.

[25] Lun, J., & Yang, L. (2016). *Experimental and Finite Element Analysis of Tire-Soil Contact Based on Tire.* Sinkage Doctoral dissertation, Northwest A&F University, Yangling, China.

[26] Zhao, Y. (2022). *Design and Experiment of Tire-soil Interaction Research Platform*. Master's Thesis, Northwest A&F University. Yangling, China. https://doi.org/10.27409/d.cnki.gxbnu.2022.000569

[27] Huang, K. (2021). *Numerical simulation of the interaction of tractor tyre with soft ground*. Master's Thesis. Jilin. University. Changchun, China. https://doi.org/10.27162/d.cnki.gjlin.2021.005385

[28] Wu, X., Xie, B., Song, Z., Shang, G., Mao, E., Li, W. (2014). Design and optimization of a single wheel tester for agricultural machinery drive tires. *Journal of China Agricultural University*. Vol.19, issue 5, pp.146-152, China. https://doi.org/10.11841/j.issn.1007-4333.2014.05.20

[29] GB/T 14828-2003. *Test method for measuring traction performance of agricultural tyres*. Beijing. Standards. Press of China. https://www.antpedia.com/standard/567682-1.html

[30] Zhu, Z., Chen, L., Xia, C., & Cai, Y. (2020). Test research on the adhesive and tractive performance of a wheeled tractor. *International journal of heavy vehicle systems*, Vol.27, issue 1/2, pp.65, China. https://doi.org/10.1504/IJHVS.2020.104425

[31] Čiplienė, A., Gurevičius, P., Janulevičius, A., & Damanauskas, V. (2019). Experimental validation of tyre inflation pressure model to reduce fuel consumption during soil tillage. *Biosystems engineering*, Vol.186, pp.45-59, Lithuania. https://doi.org/10.1016/j.biosystemseng.2019.06.023